OPTICAL METHODS FOR SIMULTANEOUS MEASUREMENT OF TEMPERATURE AND CONCENTRATION POLARIZATION

Authors: *A. Kroiß, S. Eyerer, J. Kuczaty, C. Thies, S. Wolf, A. Präbst, M. Spinnler, T. Sattelmayer*

Presenter: Alexander Kroiß
Research and Teaching Assistant – Lehrstuhl für Thermodynamik, Technische Universität München – Germany
kroiss@td.mw.tum.de

Abstract

In membrane desalination, the phenomenon of concentration polarization is the fundamental base of a variety of other effects influencing membrane performance, which is extensively discussed in literature, e.g. scaling and fouling. The experimental research on directly measuring concentration polarization is mainly based on micro-electrodes or optical methods while the latter has the advantage of being an in-situ technique without disturbing the measured phenomenon. Optical methods like Shadowgraphy, Schlieren or (Digital) Holographic Interferometry have been employed in different variations measuring the second-, first- or zeroth-order derivative of the refraction index in the investigated solution. The refraction index, however, depends not only on the concentration but also on the temperature, which is assumed to be constant throughout most published research. As the influence of temperature differences of only few K on the refraction index is in the same order of magnitude as concentration differences of few g/kg, especially in reverse osmosis and membrane distillation, it should be an aim to be able to resolve both concentration and temperature polarization simultaneously.
There are optical methods, which are capable of simultaneous investigation of heat and mass transfer boundary layers, such as two-wavelengths Holographic Interferometry. The experimental requirements on accuracy and alignment of equipment are even higher in comparison to single-wavelength Holographic Interferometry. In this work, three alternative approaches are presented and compared in view of measurement accuracy and applicability of the proposed algorithms for quantitative evaluation in post-processing. These are two-wavelengths Schlieren, single-wavelength Digital Holographic Interferometry and combined single-wavelength Digital Holographic Interferometry with Laser-Schlieren.
The present study is focused on concentration and temperature polarization in reverse osmosis and membrane distillation; however, the findings about optical methods are not limited to these desalination technologies.

I. INTRODUCTION

1.1 Temperature and Concentration Boundary Layers in Membrane Desalination

Using optical methods for measuring concentration polarization, the effect of changing refraction index within the concentration boundary layer is exploited. However, the refraction index n is also sensitive to a change in temperature (cf. figure 1), which might have an effect in the same order of magnitude as a change is salt concentration.

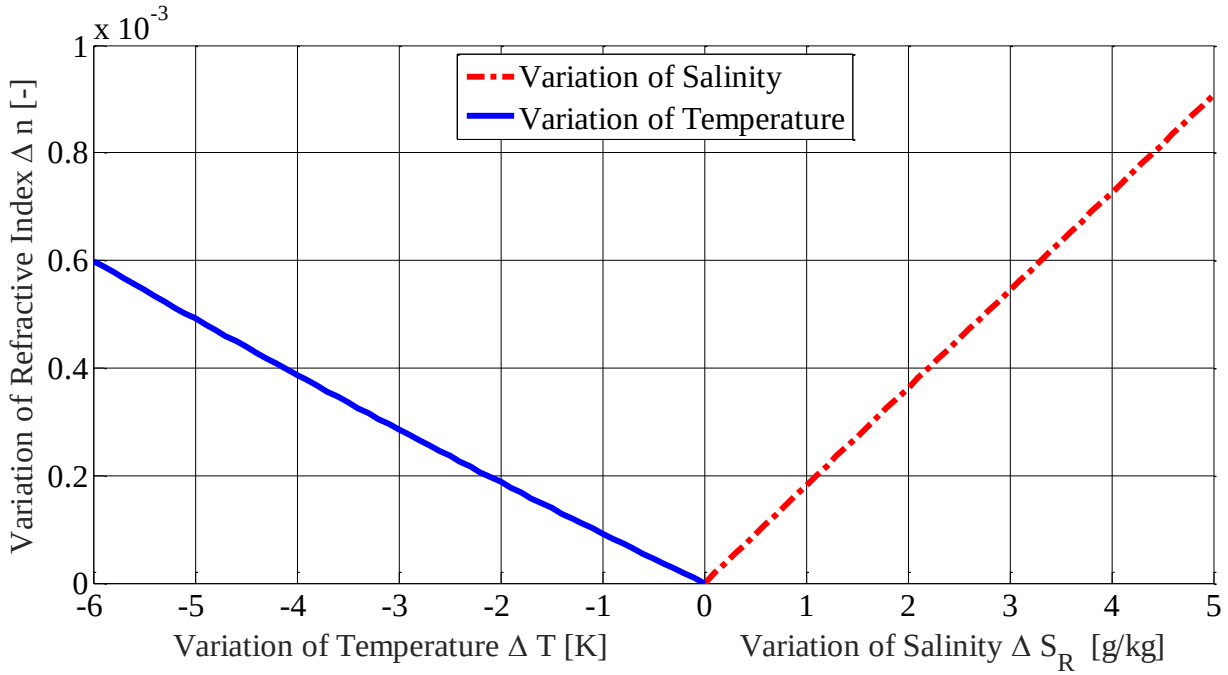

Figure 1: Influence of salt concentration and temperature variations on the refraction index of seawater – variations in temperature referred to 20°C and variations in salinity referred to 10 g/kg at 1 bar and 589.3 nm according to data of Millard and Seaver [1].

The data presented in figure 1 are based on an empirical equation of Millard and Seaver [1]. They provide nonlinear polynomial function for the refractive index of seawater depending on concentration, temperature, wavelength and pressure.

1.1.1 Reverse Osmosis

In order to investigate concentration polarization adjacent to the membrane in reverse osmosis (RO) with optical methods, the fluid temperature has to be maintained either constant in the direction perpendicular to the membrane or it has to be measured along that direction. Even if constant temperature could be guaranteed in a reverse osmosis test cell, the term "constant" has to be defined due to measurement errors and limitations of the test rig. Typical concentration polarization moduli are in the range of 1.1 to 1.2 meaning 20 % increase of concentration towards the membrane compared to the bulk phase. An increase of 10 % in salinity compared to a bulk concentration of 10 g/kg, which is typical for brackish water, means an absolute change in salinity of 1 g/kg. For seawater, this increase in concentration influences the refractive index likewise a decrease in temperature of 2 K (see figure 1, showing data provided in [1]). To be able to neglect the temperature influence, its effect on the

measured parameter, here the refraction index, has to be at least one order of magnitude lower than the concentration itself. For this example, maximum fluctuations in temperature within the investigated solution of ± 0.1 K are allowed. If the salt bulk concentration in the solution is lower, the temperature restrictions are even more rigid, while for higher concentrations it is the opposite. Furthermore, not only the bulk temperature of the feed has to be maintained within this temperature range, but also the difference in temperature between bulk and membrane need to meet these restrictions to avoid overlapping concentration and temperature boundary layers. If the membrane test cell is not totally insulated to the ambient and the test periods are not long enough to avoid temperature heterogeneity in the test cell, negligible influence of temperature in the boundary layer is hard to guarantee without high experimental effort; this is especially valid for small changes in salinity from bulk phase to membrane (a few g/kg). Investigation of transient phenomena changing operating parameters like mass flow rate, pressure and temperature are in most cases not possible as changing mass flow rates or pressures always would result in a different behavior of the operating system pump accompanied by a changed heat input into the investigated solution.

1.1.2 Membrane Distillation

In membrane distillation (MD), temperature polarization is more interesting than concentration polarization. The temperature polarization coefficient $\tau = \frac{T_{m1}-T_{m2}}{T_{b1}-T_{b2}}$ relates the temperature difference between both sides of the membrane, $T_{m1} - T_{m2}$, i.e. the driving force for the MD process, to the temperature difference between the bulk phases of the feed and distillate flow, $T_{b1} - T_{b2}$. Typical bulk temperature differences for MD are about 10 K [2]. According to Martínez-Díez and Vázquez-González [3], typical values for τ range between 0.4 and 0.7 implying a minimum temperature difference between bulk and membrane wall of 15 % of the total bulk temperature difference of 10 K, which is 1.5 K. This temperature difference results in a change of concentration of about 0.4 g/kg which is 4 % of a 10 g/kg NaCl solution. Concentration polarization of 4 % is a realistic value referring to Martínez-Díez and Vázquez-González [3], who investigated temperature and concentration polarization for NaCl solutions between 0 and 100 g/kg. The refraction index of a NaCl-water solution is very similar to the one of seawater. Although concentration polarization does not have a major effect on the distillate production in MD, optical methods do have to take it into account as its effect on the refraction index is in the same order of magnitude as the temperature polarization effect.

1.2 Fields of Application

There are different reasons why boundary layer measurements in membrane desalination are necessary. An obvious one is to predict the physical state of the fluid directly at the membrane which is fundamental for the driving force of the overall process. Current research goes beyond the mere empirical description and theoretical modeling of boundary layer phenomena, like temperature and concentration polarization. Understanding both phenomena is the basis for further research like on module or spacer geometry design but also on scaling and fouling phenomena. Another advantage of boundary layer measurements might be the determination of local membrane characteristics. The hypothesis is that the boundary layer is unique to its problem, defined by flow regime, material properties, temperature, bulk concentration and pressure on both sides of the membrane, as well as the membrane itself. Based on the zeroth-, first- and second-order derivative of the concentration at different positions in the boundary layer, the local membrane properties, the local permeate mass flow rate and the local permeate concentration can be measured [4].

1.3 Scope of the Paper

As mentioned above, simultaneous measurement of concentration and temperature boundary layers can be motivated in different fields of membrane desalination. The aim of this work is to give an overview of currently available experimental methods and to point out the drawbacks of the state-of-the-art. Subsequently, three promising strategies are presented to avoid these disadvantages. These are two-wavelengths Schlieren, single-wavelength Digital Holographic Interferometry and combined single-wavelength Digital Holographic Interferometry with Laser-Schlieren. The approaches differ in the experimental requirement on accuracy and alignment of equipment. They are compared in view of measurement accuracy and applicability of the proposed algorithms for quantitative post-processing.

II. LITERATURE REVIEW

There are different optical methods to determine the refraction index of a fluid in boundary layers. The three main types are: Shadowgraphy, a technique to measure the second derivative of the refraction index; Schlieren, a technique to measure the first derivative of the refraction index; and Interferometry, a technique to measure the refraction index directly. While the techniques measuring derivatives of the refraction index (Shadowgraphy and Schlieren) have the generic disadvantage that the determined data, and thus measurement errors, have to be integrated to get the refraction index, they are easier to implement experimentally. In the following, a brief overview of the application of optical methods in desalination and in other fields to determine heat and/or mass transfer boundary layers is given.

2.1 Boundary Layers in Membrane Desalination

Chen et al. [5, 6] provided a review for the state-of-the-art, in 2004, about in situ monitoring techniques for concentration polarization and fouling phenomena in membrane processes including optical methods. They pointed out the advantage of non-destructive measurements with the principle option of real time investigations for all optical techniques. All of the cited methods, however, do not take into account the influence of temperature deviations on the measured concentration boundary layer.

Vilker et al. [7, 8] started the research on boundary layers with optics in the field of membrane desalination. They applied Shadowgraphy managing to measure the concentration boundary layer to about 200 µm above an RO membrane in the 1980s. Despite the impression often given in literature, it has to be mentioned that the Shadowgraphy method itself is not restricted to this resolution of 200 µm, which is more related to the specific design of the experiment conducted. Since the publications of Vilker et al. [7, 8], no other report has been found about application of Shadowgraphy in desalination.

As far as is known, the Schlieren technique has not been applied at all in membrane desalination. Instead, the interference methods gain higher popularity. Johnson [9] and Mahlab et al. [10] started with conventional interferometry up to 1980, while the trend towards Holographic Interferometry (HI) was introduced by Clifton and Sánches [11] in electrochemical cells, in 1979, and later, in the end of the 1990s, continued and further developed by Fernández-Sempere et al. [12-17] and Salcedo-Díaz [18] until 2010, with a focus on ultrafiltration (UF) but also on RO. Rodrigues et al. [19] picked up again the challenge of ray-tracing in 2013, which was investigated already by Beach et al. in 1973 [20], while Fernández-Sempere et al. [17] and Salcedo-Díaz [21] conducted the first experiments applying Electronic Speckle Pattern Interferometry (ESPI) in RO desalination, which is similar but not the same as Digital Holographic Interferometry (DHI). The main difference between an ESPI and a DHI optical

setup is an imaging lens system, which allows focusing only on one defined object plane. In case of ESPI, the hologram plane and image plane are identical; the recorded image can be referred as image plane hologram, i.e. the hologram of a focused image [22]. Thus digitally focusing on different objects planes is only possible with DHI and not its derivate ESPI.

Growman and Either [23] presented one of the rare publications about measuring both the refraction index and its gradient by layer beam deflection across and above the membrane area in 1997. The investigated object was the concentration boundary layer in an UF batch-cell. The information of the zeroth- and first-order derivative is used to achieve higher measurement accuracy, but not to study two different boundary layers simultaneously.

Accompanied by the optimization of the measurement technique, the investigated objects changed throughout the years from batch-cell to more realistic cross-flow experiments as well as from steady-state to dynamic experiments. In view of applied pressures, the tests at maximum pressure of 30 bar by Mahlab et al. [10] have not been exceeded yet.

2.2 Boundary Layers in General

While optical methods for investigating refractive index fields are comparably rare in membrane desalination, they are well known and frequently applied in other disciplines, especially the conventional forms of Shadowgraphy, Schlieren and Interferometry. Therefore, this overview of generic investigations of boundary layers is focused on the simultaneous, quantitative resolving of two or more influencing parameters on the refraction index.

One of the few examples for two-wavelengths Schlieren is the work of Prevosto et al. [24, 25]. They used the quantitative Schlieren technique for measurements in plasma with two lasers with wavelengths of 632.8 nm and 514 nm, respectively, to be able to resolve electron and gas densities. The uncertainties for both investigated parameters were around 30 % and 60 % for the electron and the gas density, respectively.

Panknin [26] applied a two-wavelengths Holographic Interferometry method to investigate heat and mass transfer boundary layers simultaneously. Although the experimental results of the temperature and concentration boundary layer of a vertical plate and a horizontal cylinder, both heated and substance releasing, provided a proof of concept, restrictions and difficulties in the alignment process of the experimental setup due to the high need of accuracy are emphasized. The attempt to resolve temperature and fuel distribution in a flame failed. Additionally, El-Wakil and Ross [27] reported not to be able to achieve a high accuracy to analyze combustion and evaporation in liquid fuels by means of heat and mass transfer boundary layers measurements with a two-wavelengths Mach-Zehnder Interferometer.

A multi-wavelengths approach in Holographic Interferometry is described by Desse and Picart [28] who investigated unsteady flows and flows with shocks. They pointed out the difficulty of identifying and counting interference fringes in monochromatic light in the context of shock waves and complex flow conditions. For quantitative measurements, the zeroth-order fringe has to be known as starting point for calculating fringes. A three-wavelengths-approach allows doing it unambiguously. They indicated that a digital approach for Holographic Interferometry (status 2012) is not practical yet due to current CCD resolutions. However, the fact that it is basically possible to do a DHI setup within the accuracy needed for the alignment of three beams with different wavelengths is promising.

While the combination of Schlieren and Interferometry has not been used to measure two boundary layers simultaneously, as far as it is known, the idea of combining both setups is not new. Already in 1957, Blue [29] patented a combined Interferometer-Schlieren apparatus for density determination in non-homogeneous transparent fields, however, not pointing out the potential of being an alternative to the two-wavelengths approach. The setup is explained in section 3.2 in more detail.

Kastell and Eitelberg [30] investigated 3D density flow fields with a combined Holographic Interferometer and Laser-Schlieren system in high temperature and high velocity flows. The reason for the application of Schlieren in addition to DHI is the disadvantage of DHI not providing a fringe shift if the light path is too short while Schlieren still gives valuable information, which is not discretized by fringes but by the pixel density on the camera chip.

In the field of MD, temperature polarization was investigated by liquid crystal thermography [31]. Thermochromic Liquid Crystals (TLCs) are very good for qualitative investigations. For quantitative investigation, however, the an accuracy of ± 0.2 °C for a resolvable temperature range of total 1°C or ± 1 °C for a resolvable temperature range of total 5°C [32] sets tight constraints to the experiment.

2.3 Discussion

Although there is a need for simultaneous measurement of temperature and concentration boundary layer in membrane desalination, an appropriate experimental method has not been found and applied yet.

In membrane desalination, the main focus is on applying interference methods, mostly HI and its derivate ESPI. Temperatures are assumed to be constant in experiments, although this might be difficult to achieve in practice, especially in boundary layers.

The potential of the Schlieren technique with regards to the two-wavelengths approach seems not to have been investigated by now, although it might be less complex in alignment of the optical setup compared to (D)HI. Furthermore, while DHI faces challenges due to low resolution of the CCD chip compared to holographic plates, (digital) Schlieren might not have this problem. Especially the development of cameras being able to record colors, e.g. in a RGB format, on a CCD chip might support the popularity of the Schlieren method.

The two- or multi-wavelengths approach in combination with Holographic Interferometry seems to be very difficult due to the high need for accuracy. Although the alignment procedure is very complex, it is possible.

Experimental setups combining Interferometry and Schlieren have been aligned successfully but a simultaneous measurement of heat and mass transfer boundary layers has not been tried yet.

Concluding the findings of the literature review, a two-wavelengths quantitative Schlieren approach as well as an evaluation based on zeroth- and first-order derivative of the refraction index, subsequently called gradient algorithm, applied in a single-wavelength DHI and a combined, single-wavelengths DHI-Schlieren setup is to be investigated to identify its potential for overcoming the drawbacks of the state-of-the-art methods applied in membrane desalination. In the following, ESPI is to be considered as a subset of the DHI and thus not discussed separately.

III. METHODS FOR SIMULTANEOUS MEASUREMENT OF TEMPERATURE AND CONCENTRATION POLARIZATION

3.1 Two-Wavelengths Schlieren

The Schlieren method is usually based on a white light source including a wide range of wavelengths. Using e.g. a single lens reflex camera with a Bayer color filter for recording the Schlieren image it is possible to make use of the wavelength dependency of the refraction index. Picking up the idea presented by Panknin [26], the information contained in the refraction of rays with two different wavelengths can be used. For the two unknown parameters, concentration and temperature, two equations are available. This makes it possible to identify both separately.
The difference between these two wavelengths should be as high as possible with the limitation that they have to be still recordable by the digital chip covered with a Bayer filter. Figure 2 shows the Schlieren setup including a double band-pass filter, transmitting only red and blue light simultaneously.

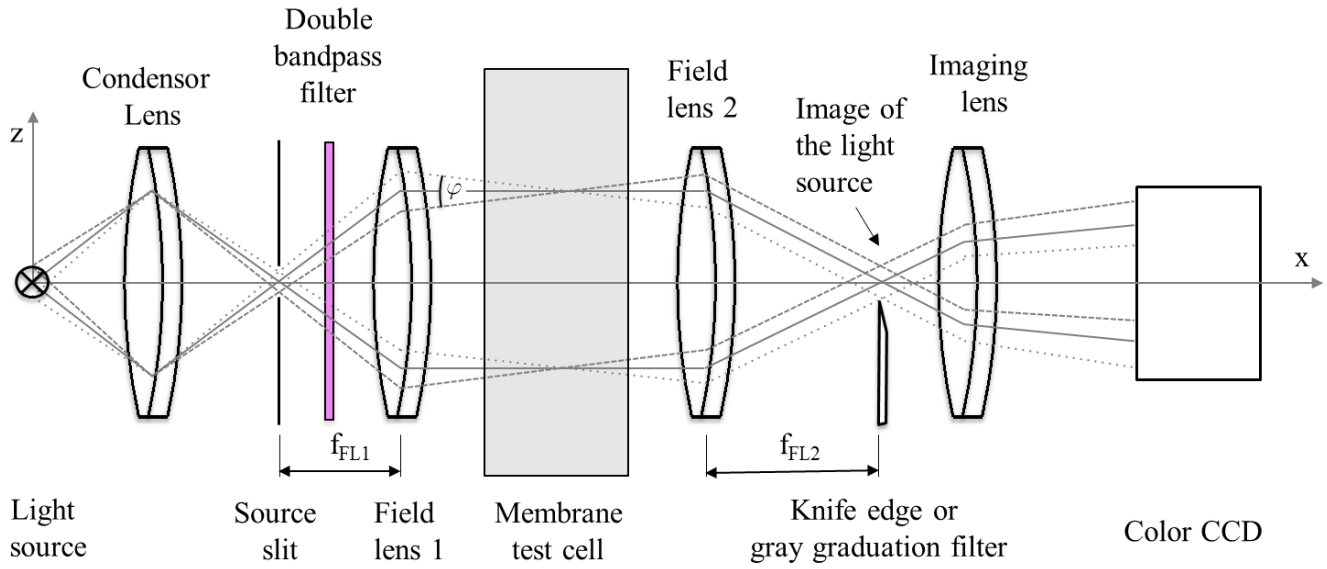

Figure 2: Two-wavelengths Schlieren setup for quantitative, simultaneous investigation of concentration and temperature boundary layers.

Figure 3 depicts the difference in the refraction index for blue and red light, which can be recorded by common single lens reflex cameras. It becomes clear that there might be the need of high measurement accuracy to resolve differences in refraction index in the order of magnitude of 10^{-5}.

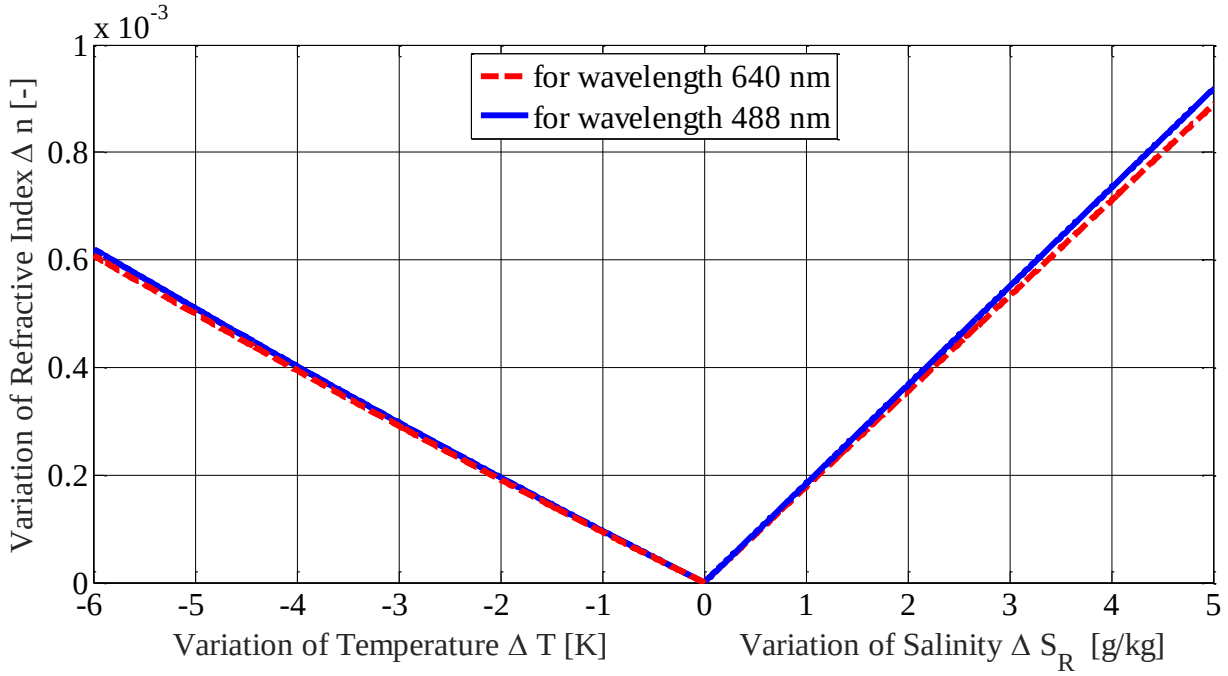

Figure 3: Difference between the refraction index for blue and red light as an indicator for the needed accuracy in the setup: measurement of the refraction index in the order of 10^{-5}. Variations in temperature are referred to 20°C while variations in salinity are referred to 10 g/kg at 1 bar, both depicted for wavelength 488 nm and 640 nm according to the data of Millard and Seaver [1].

3.2 Improved Single-Wavelength Digital Holographic Interferometry

Provided that the refraction index as a function of the investigated influencing parameters, in our case concentration and temperature, is known, it is claimed that it can be avoided to rely on two-wavelengths applying HI for simultaneous heat and mass transfer boundary layers. To be able to resolve two unknown parameters, temperature and concentration, a set of two equations is needed for the refraction index which is solvable (e.g. determinant of Jacobi matrix is not equal to zero). The idea, proposed in this work, is to make use of the first- and zeroth-order derivative of the refraction index.

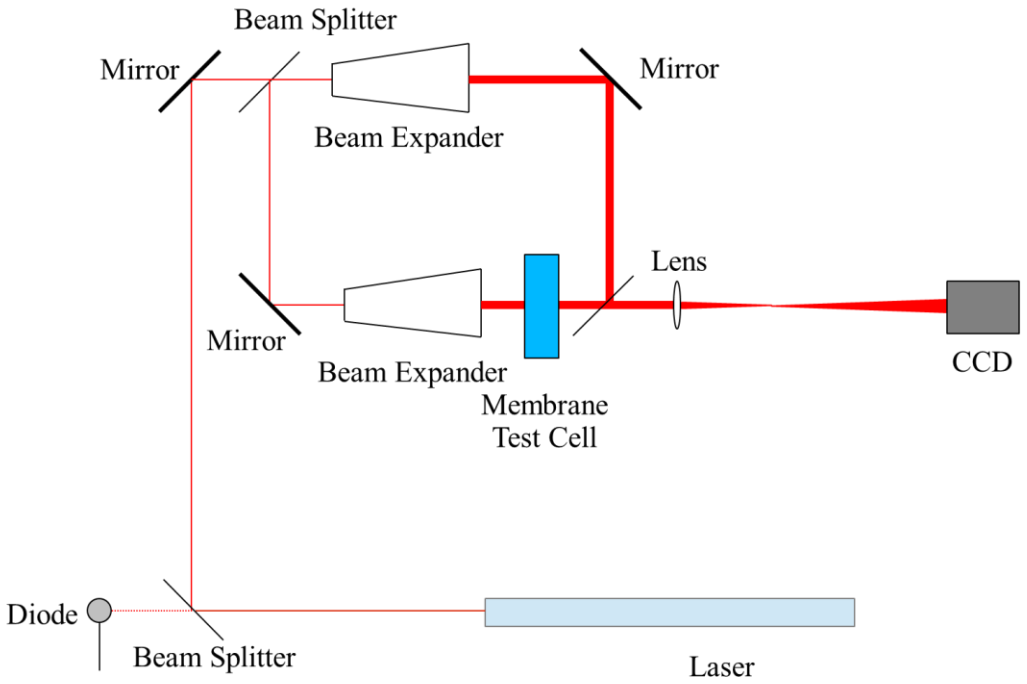

Figure 4: Single-wavelength Digital Holographic Interferometry setup.

Holographic Interferometry provides information about the refraction index at different positions above the membrane. The function of the refraction index depending on position is obtained counting fringes starting from the bulk phase to the considered position. In the end, the zeroth-order derivative of the refraction index is known. Afterwards, the first-order of the refraction index depending on the position above the membrane can be derived. The empirical correlation of the refraction index depending on temperature and concentration can be differentiated with respect to the position above the membrane as follows:

$$a_0 + b_1 T + b_2 T^2 + \cdots + d_1 c + d_2 c^2 + \cdots + e_1 T c + e_2 T^2 c + e_3 T c^2 + e_4 T^3 c + \cdots = n \qquad (1)$$

The polynomial function with different orders of concentration and temperature and known coefficients $a_i, b_i, d_i, e_i, \ldots$ becomes after differentiating:

$$0 + b_1 \frac{dT}{dz} + 2b_2 T \frac{dT}{dz} + \cdots + d_1 \frac{dc}{dz} + 2d_2 c \frac{dc}{dz} + \cdots + e_1 \frac{dT}{dz} c + e_1 T \frac{dc}{dz} + 2e_2 T \frac{dT}{dz} c + e_2 T^2 \frac{dc}{dz} + e_3 \frac{dT}{dz} c^2 + 2e_3 T c \frac{dc}{dz} + 3e_4 T^2 \frac{dT}{dz} c + e_4 T^3 \frac{dc}{dz} \ldots = \frac{dn}{dz} \qquad (2)$$

Per se, the derivatives of temperature, $\frac{dT}{dz}$, and concentration, $\frac{dc}{dz}$, are not known. However, considering how those derivatives would be calculated numerically, they are substituted by finite differences. Here a two-point backward difference scheme, $\frac{T_i - T_{i-1}}{\Delta z}$ and $\frac{c_i - c_{i-1}}{\Delta z}$ is exemplarily applied. To be able to calculate the refraction index course for the entire profile, for each discretization step temperature and concentration have to be calculated step by step.

Starting at the bulk phase, temperature and concentration can be derived for the position of the first fringe I as the parameters in the bulk phase are known (step 1: *i* stands for the first fringe, and *i*-1 stand

for the bulk phase). Analogously, in step 2, the state of the second fringe (II) can be calculated from the parameters of fringe I, which are known now, and so on for all other fringes. The generic equations for step i are:

Step i, fringe (i-1) to fringe (i):

$$a_0 + b_1 T_i + b_2 T_i^2 + \cdots + d_1 c_i + d_2 c_i^2 + \cdots + e_1 T_i c_i + e_2 T_i^2 c_i + e_3 T_i c_i^2 + e_4 T_i^3 c_i + \cdots = n_i \tag{3}$$

$$\begin{aligned} 0 + b_1 \frac{T_{i-1} - T_i}{\Delta z} + 2 b_2 T_i \frac{T_{i-1} - T_i}{\Delta z} + \cdots + d_1 \frac{c_{i-1} - c_i}{\Delta z} + 2 d_2 c_i \frac{c_{i-1} - c_i}{\Delta z} + \cdots \\ + e_1 \frac{T_{i-1} - T_i}{\Delta z} c_i + e_1 T_i \frac{c_{i-1} - c_i}{\Delta z} + 2 e_2 T_i \frac{T_{i-1} - T_i}{\Delta z} c_I + e_2 {T_i}^2 \frac{c_{i-1} - c_i}{\Delta z} \\ + e_3 \frac{T_{i-1} - T_i}{\Delta z} c_i^2 + 2 e_3 T_i c_i \frac{c_{i-1} - c_i}{\Delta z} + 3 e_4 {T_i}^2 \frac{T_{i-1} - T_i}{\Delta z} c_i + e_4 {T_i}^3 \frac{c_{i-1} - c_i}{\Delta z} \ldots \\ = \frac{n_{i-1} - n_i}{\Delta z} \end{aligned} \tag{4}$$

Equations (3) and (4) are two discretized equations which allow to determine the two unknown parameters T_i and c_i.

A challenge to this method might be interference measurements with few fringes leading to a high, insufficient step size and, consequently, poor accuracy. Furthermore, the advantage of HI compared to Schlieren method, not relying on the foregoing discretization step when evaluating the refraction index of interest, is gone. The cost of resolving both temperature and concentration is therefore accuracy of the method compared to conventional HI.

3.3 Combined Single-Wavelength Digital Holographic Interferometry with Laser-Schlieren

The drawbacks of the previously described method might be significantly reduced by a combination of the Schlieren technique with Digital Holographic Interferometry. While DHI provides supporting points for the evaluation of Schlieren, Schlieren provides continuous information about the first-order of the refraction index. The discretization step is not limited any more to the fringe positions. This might have a significant influence on the accuracy of the method. Another advantage is the rather simple integration of the Schlieren setup in a quasi-inline DHI setup. After the test cell, see figure 5, the object beam is split, half of it proceeds to the Laser-Schlieren setup and the other half is united with the reference beam in a beam splitter and then recorded digitally with a second camera. Due to the DHI setup, parallel light is guaranteed in front of the test object, which is required for the Schlieren method also. Thus the alignment of the Schlieren equipment is rather easy. To achieve the same magnification in the DHI and Schlieren setup, a lens-system is needed. In preliminary experiments it was found that a weak point of the setup is the coupling of the two beam splitters after the beam expanders, which makes it more difficult to align the DHI part. Very promising, however, was the Laser-Schlieren result itself. The quality of the Schlieren image could have been significantly reduced by diffraction patterns appearing in the image due to unavoidable disturbances in the optical setup (dust on lenses, dirt on test cell windows). In the preliminary experiment it was observed that the influence of these diffraction patterns is small due to the rather high magnification of the image which is necessary when investigating boundary layers.

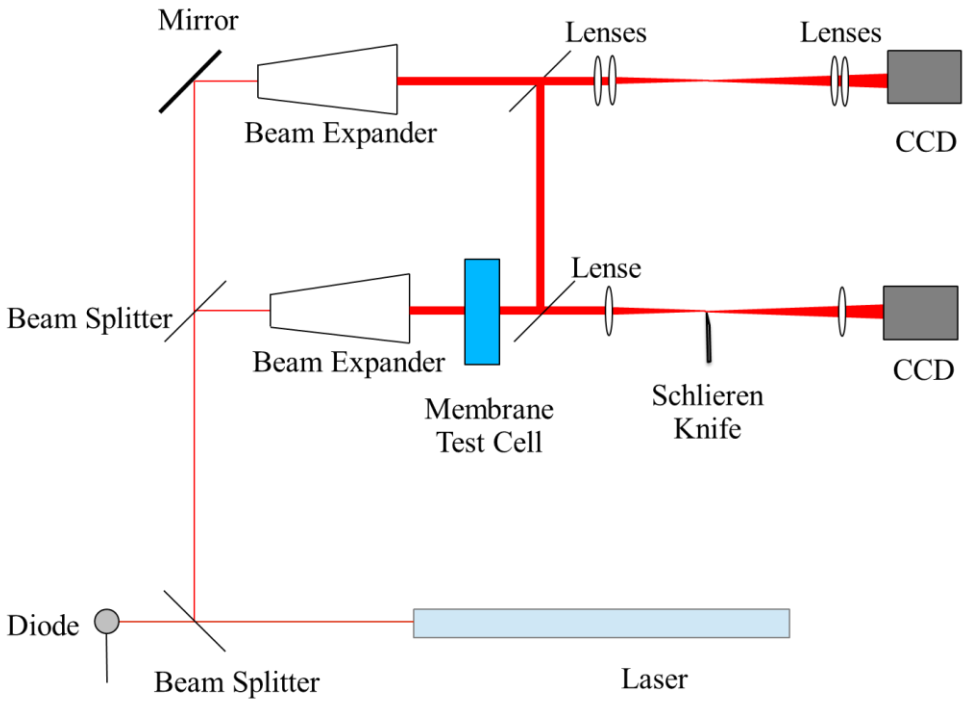

Figure 5: Combined Single-Wavelength DHI with Laser-Schlieren setup, similar to the patented setup of Blue [29].

IV. POTENTIAL ANALYSIS OF PROPOSED METHODS

In order to estimate the potential of the proposed methods, both measurement accuracy and the algorithm for quantitative data evaluation are critical to their success. In the following, it is attempted to give a quantitative estimation of the measurement accuracies. Based on this, an outlook on the applicability of the proposed methods is given.

4.1 Measurement Accuracy

In order to investigate the measurement accuracy of the proposed methods, RO experiments were conducted with a two-wavelengths Schlieren and a DHI (ESPI) setup at almost identical operating conditions (± deviation ranges between Schlieren and DHI are given in table 1):

Table 1: Operating Parameters

Parameter	Value	Ranges for Difference between Schlieren and DHI Experiment
Pressure	13 bar	± 1 bar
Bulk-temperature	20°C	± 1 °C
NaCl bulk-concentration	10 g/kg	± 0.5 g/kg
Mass flow rate	10 l/h	± 0.5 l/h
Feed channel dimensions (Width x Length x Height)	10 x 180 x 60 mm³	
Reynolds Number	79	± 4

As the optical methods differ in the measured quantity, which is ray deflection in case of Schlieren and phase shift in case of DHI, it was tried to find a common base for comparison: the refraction index and the refraction index gradient. As it will turn out later, the order of magnitude of measurement accuracy and noise of both quantities is decision making for the success of the numerical post-processing. Therefore, the following analysis will focus on the order of magnitudes and generic trends.

The measurement error estimation is done exemplarily for a concentration profile as depicted in figure 6. Both the Schlieren and the DHI experiment were conducted such to gain a high concentration polarization with a modulus of 1.7 ($= \frac{w_M}{w_F}$). In this case the temperature needs to be maintained constant in a range of ± 1 K to be negligible. This is achieved by a long operation time (several hours) in steady-state conditions at the same fluid and ambient temperature before the actual experiment starts (the bulk temperature deviations given in table 1 refer to differences between Schlieren and DHI, not to variations of the bulk temperature in the experiment itself).

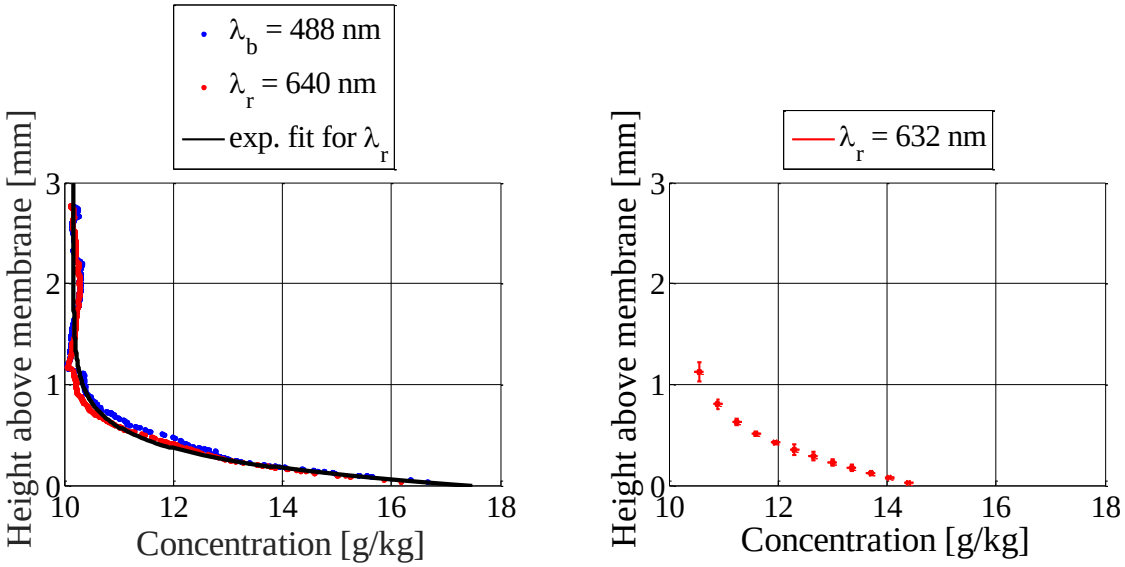

Figure 6: Concentration boundary layer measurement with two-wavelength Schlieren (left) and single-wavelength DHI (right).

The results of the Schlieren and the DHI experiment are in good agreement. The concentration boundary layer heights are comparable (~ 1.2 mm) while concentration directly on the membrane differ most. In case of Schlieren, the difference between the red and the blue wavelength measurement serve as an indicator for the measurement accuracy. Moreover, the difference is also an indicator for temperature influence on the refraction index gradient measurement: if the concentration profiles for both wavelengths are identical, temperature influence can be neglected; this is the case here. While the Schlieren evaluation is based on one single image, 50 successive images were recorded at the same state of the experiment in case of DHI. The standard deviation of this image series serves as an indicator for the DHI measurement accuracy.

The Schlieren concentration profile is obtained from light ray deflection measurements, which contain information about the first-order derivative of the refration index profile. Thus an integration step is necessary to derive the refraction index profile. With the correlation from Millard and Seaver [1], the refraction index data are converted to concentration data.

Instead, the DHI profile is based on data for the refraction index, which do not have to be integrated from refraction index gradient data but are directly measured; thus, measurement error propagation due to integration is only a problem for the Schlieren method.

In order to be able to give an error estimation for the refraction index measured with the Schlieren method, we start with differentiating an exponential curve fit of the refractive index profile corresponding to the concentration profile presented in figure 6, left. Thus, an artificial, ideal curve for the refractive index gradient for Schlieren is gained. Then noise is added to this ideal, analytical profile. The noise is designed similar to the one observed in preliminary experiments. A Gaussian distribution was found to fit well. As the mean value of the noise of the refraction index gradient is the reason for error propagation when integrating to obtain the refraction index, one best and two worst case scenarios are defined. The best case assumes a mean value of the Gaussian distribution of zero, while the worst cases are designed with ± three times the mean value of the dn/dz distribution ($-1.3 \cdot 10^{-5}\,\frac{1}{\mathrm{mm}}$) derived from the conducted Schlieren experiments (figure 7, left). Based on these three cases, the refraction index is calculated. An envelope is defined by the worst case scenarios in which the real refractive index profile is supposed to lie (figure 8, left).

As already mentioned, the error of the DHI refraction index measurements is estimated by the standard deviation derived from 50 successive images. For a better understanding, its physical background is explained shortly: the main error results from vibrations of the RO test rig, caused by the low and high pressure pumps. First of all, vibrations lead to displacements of the fringes, accounted by the standard deviation of the fringe position above the membrane. Second, vibrations might lead to a change in the total amount of fringes since the frist fringe appearing close to the bulk phase might vanish. As the measurement of the refraction index is based on counting the fringes starting from the bulk phase, this directly affects the refraction index value of the considered fringe, taken into account by a standard deviation of the refraction index value (figure 8) and concentration (figure 6), respectively. For the presented example this means: 12 fringes can be observed in 43 of 50 images (86 % of 50 images). The standard deviation for the fringe position is calculated only for the cases when all 12 fringes are visible. To take account for the remaining 14 % of the 50 images, the differerence in refractive index between two fringes (in this example $\Delta n = 6.32 \cdot 10^{-5}$), which is the maximum error for the refractive index value, is tried to be referred to an equivalent to a standard deviation measure: with ± 0.5 Δn, 86% of the measurements are covered. To gain an equivalent to a three sigma band (± 3σ) of a Gaussian distribution, 99.7% of all data need to be taken into account, thus ± 0.5 $\Delta n \cdot \frac{0.997}{0.86}$. It results a standard deviation equivalent of the refractive index of a fringe:
$\sigma_n = \pm \frac{1}{3} \cdot 0.5\,\Delta n \cdot \frac{0.997}{0.86} = 1.22 \cdot 10^{-5}$.

It should be noted that vibrations can only be minimized but never avoided, as the pumps are system-inherent in membrane desalination. The measurements were conducted without a vibration-stabilized optical table, which is not seen to be helpful as the measurement object, the membrane test cell, is connected to the hydraulic circuit anyway. Thus, it was rather attemped to align the setup such that existing vibrations are the same for test cell, optical equipment and camera.

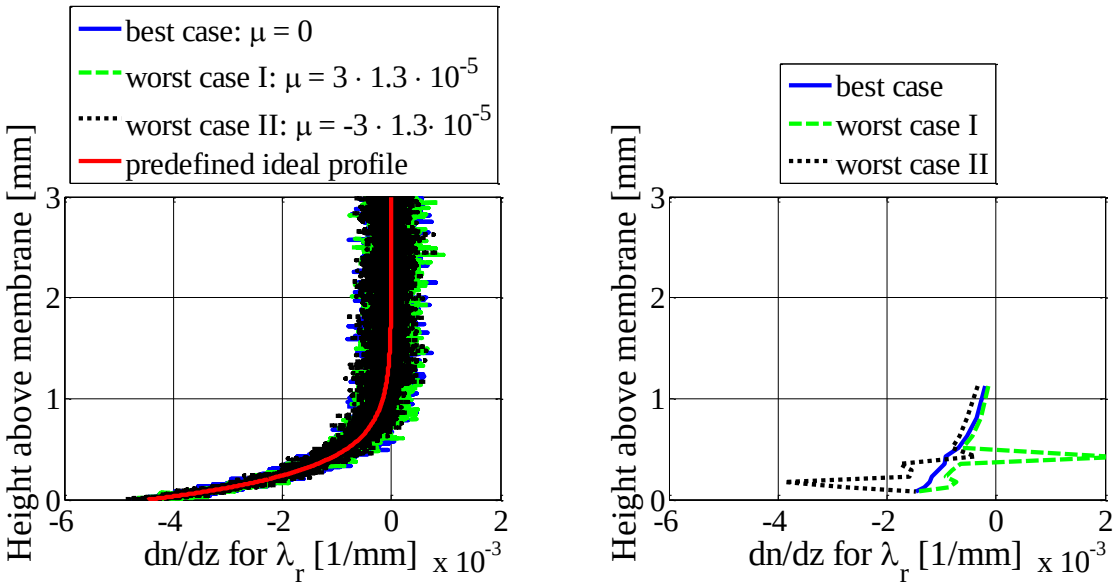

Figure 7: Estimation of measurement accuracy for refractive index gradient determined with Schlieren (left) and DHI (right).

In order to be able to compare the accuracies of the refraction index gradient measurements, the refraction index profile of the DHI measurement has to be differentiated. This is done with forward finite differences taking into account a three sigma band ($\pm\ 3\sigma$) as maximum deviation for both the refractive index values itself as well as the *z*-position values of the fringes (see figure 7):

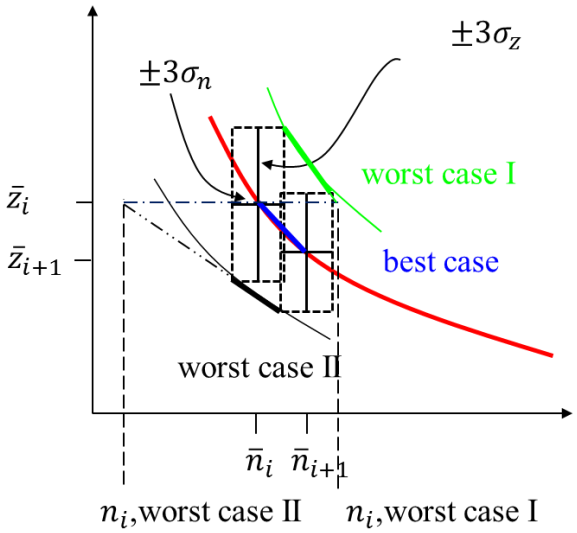

Figure 7: Approximations for "best case", "worst case I" and "worst case II".

$$\left.\frac{dn}{dz}\right|_{i_{\text{worst case,I}}} = \frac{\bar{n}_{i+1} - \bar{n}_i}{(\bar{z}_{i+1} + 3 \cdot \sigma_{z,i+1}) - (\bar{z}_i + 3 \cdot \sigma_{z,i})} \tag{5}$$

$$\left.\frac{dn}{dz}\right|_{i_{\text{best case}}} = \frac{\bar{n}_{i+1} - \bar{n}_i}{\bar{z}_{i+1} - \bar{z}_i} \tag{6}$$

$$\left.\frac{dn}{dz}\right|_{i_{\text{worst case,II}}} = \frac{\bar{n}_{i+1} - \bar{n}_i}{(\bar{z}_{i+1} - 3 \cdot \sigma_{z,i+1}) - (\bar{z}_i - 3 \cdot \sigma_{z,i})} \tag{7}$$

The numerical method of differentiation has an influence on the determined gradient; however, to be able to give an estimate of the order of magnitude, the forward finite differences scheme is seen to be satisfactorily here. The worst cases are designed to take into account that the fringes do oscillate due to vibration, but all together in the same direction. Between two fringes, the difference in refraction index does not change. Consequently, worst case I represents the case when all fringes oscillate to their maximum position above the membrane while they reach their minimum position in worst case II. As seen already during the Schlieren analysis, an envelope is defined by these two worst cases.

Both refractive index gradients are in the same order of magnitude. Comparing the envelopes defined by extreme values of the measurement noise, in case of Schlieren, and the minimum and maximum value of the derived refraction index gradient (worst case I and II), in case of DHI, it can be concluded that the accuracy along the coordinate perpendicular to the membrane remains the same for Schlieren ($\pm$ 0.6 10^{-3}) while it seems to decrease towards the membrane for DHI. As the standard deviation of the refraction index, σ_n, is constant for DHI, the refraction index error term, represented by σ_n, only becomes dominant over the deviation in *z*-direction, σ_z, for small differences between the fringes, i.e. close to the membrane. Assumed a monotone decrease of σ_z from bulk phase to membrane, which is expected when only vibrations are disturbing the measured signal, actually a confining envelope might be expected for DHI as long as σ_z dominates σ_n. However, the presented example is based on real experimental data which do not show a clear monotonous decrease of σ_z resulting in rather an undefined shape of the envelope.

Compared to a DHI setup, in which the data discretization is limited to the number of fringes, Schlieren has the advantage of many sampling points (as many as pixels on the camera chip).

The refraction index and its envelope of accuracy, defined by the worst case scenarios for Schlieren and the standard deviations for DHI, are depicted in figure 9 for both Schlieren and DHI.

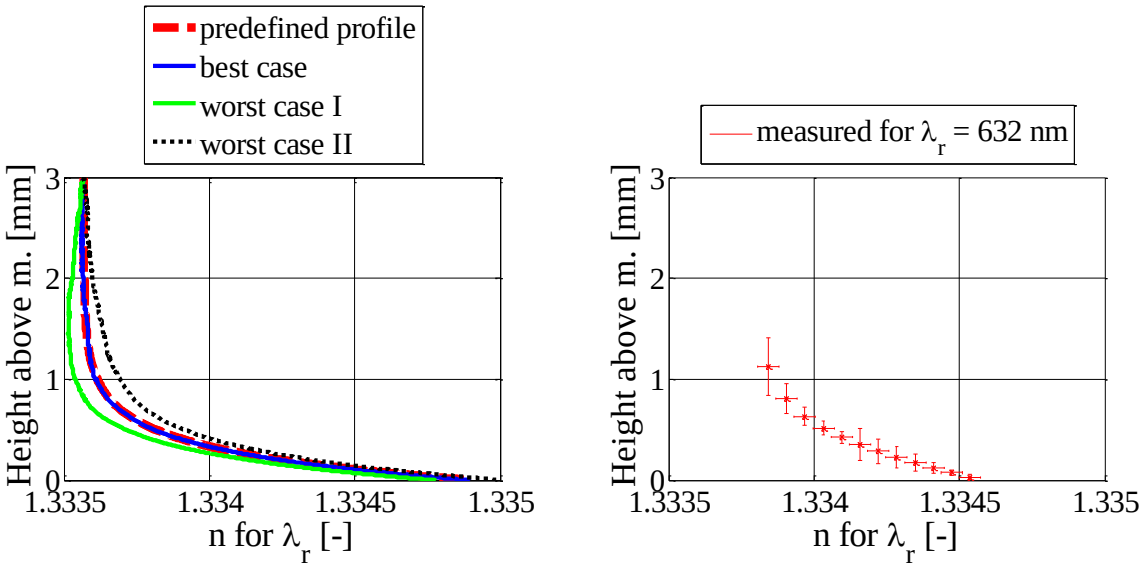

Figure 9: Estimation of measurement accuracy for refractive index determined with Schlieren (left) and DHI (right) – refraction index profiles. For DHI, the 3σ-band is depicted.

The differences between the different scenarios for the measurement data depicted in figure 9 are illustrated in more detail in figure 10. In case of Schlieren, this is a simple subtraction of the data. In case of DHI, the influence of both deviations, position and refraction index value, have to be taken into account. This is estimated by linear interpolation within the 3σ-band of the data:

$$n_{i_{\text{worst case,I}}} = \bar{n}_i + 3 \cdot \sigma_n - 3 \cdot \sigma_{z,i} \left.\frac{dn}{dz}\right|_{i_{\text{worst case,I}}} \tag{1}$$

$$n_{i_{\text{best case}}} = \bar{n}_i \tag{2}$$

$$n_{i_{\text{worst case,II}}} = \bar{n}_i - 3 \cdot \sigma_n + 3 \cdot \sigma_{z,i} \left.\frac{dn}{dz}\right|_{i_{\text{worst case,II}}} \tag{3}$$

The accuracy of the refraction index measurement decreases towards the membrane for the Schlieren method. This was already indicated above: when the mean value of the noise distribution of the refraction index gradient measurement is not zero, it is integrated from the bulk phase towards the membrane, i.e. the error is increased. In case of DHI, it is difficult to identify a clear trend; it seems that there is a minimum difference between the different cases (about $1 \cdot 10^{-4}$), which is only exceeded when the standard deviations for the fringe height position is not following the trend of monotone decrease from bulk phase to membrane. Directly at the membrane, high values of accuracy can still be reached for DHI.

Comparing Schlieren and DHI, the absolute value for refraction index accuracy is interesting – in this analysis, Schlieren can compete with DHI. The main reason might be the negative influence of vibrations on the DHI results which might not be of such relevance for Schlieren experiments.

Furthermore, the result is quite promising as the required accuracy for two-wavelengths Schlieren of 10^{-5} (cf. figure 3) seems to be achievable according to the best case scenario.

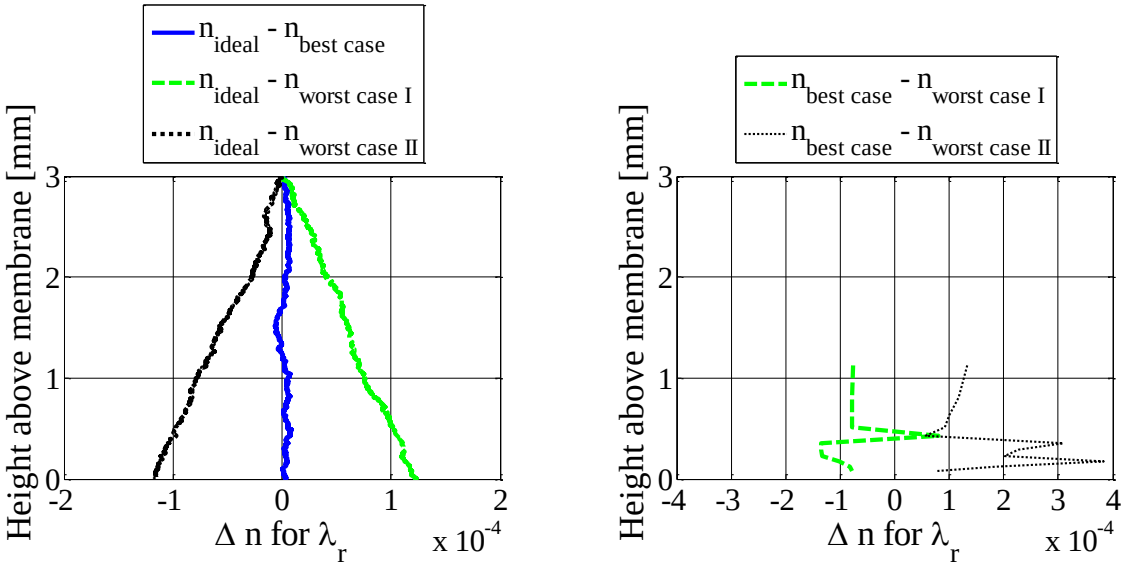

Figure 10: Estimation of measurement accuracy for refractive index determined with Schlieren (left) and DHI (right) – order of magnitude of measurement error.

Concluding the findings of the analysis of accuracy, it is interesting that the trend of the measurement accuracy is different for Schlieren and DHI. The hypothesis that the combination of both might be promising is supported.

4.2 Numerical Evaluation – Critical Needs of Algorithms

4.2.1 Two-Wavelength Algorithm

As the refraction index of seawater is only a weak function of wavelength, it is important to identify the required measurement accuracy. As mentioned already, Millard and Seaver [1] provide an empirical, nonlinear polynomial function for the refractive index of seawater depending on concentration, temperature, wavelength and pressure. That this function is appropriate for application to the current problem of two-wavelengths Schlieren is to be exemplarily shown in the following.

First, a concentration and a temperature profile chosen from experimental data and fitted by exponential functions serve as ideal reference profiles: For the concentration profile, the example from above (chapter 4.1) used, while for the temperature profile available data for a bulk phase temperature of 27.2 °C are taken. From those ideal data, the refraction index is calculated and its gradient as well as deflection data are derived. Then concentration and temperature are re-calculated starting from the deflections again, as it is to be done just as with experimental data. This easy task is solved appropriately as can be seen in figure 11.

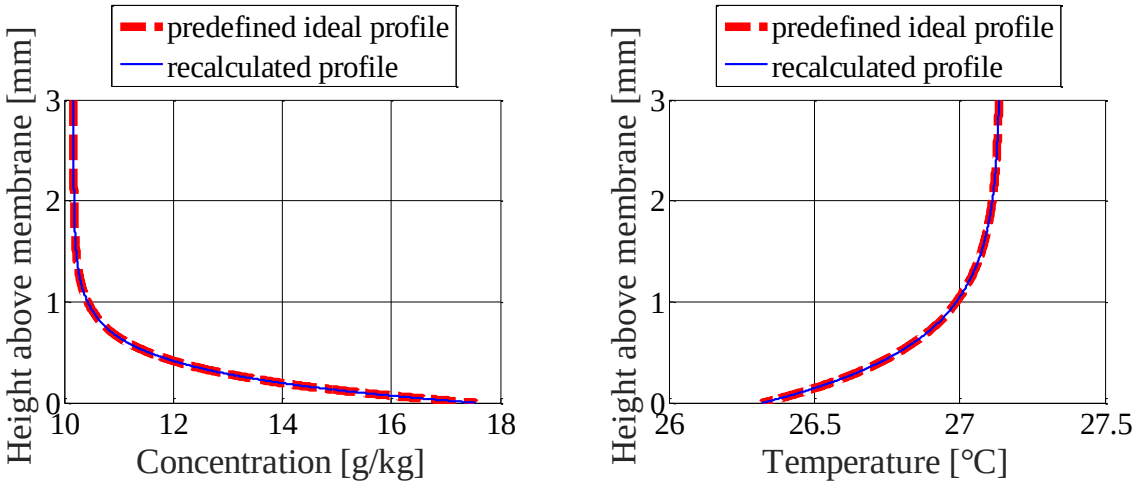

Figure 11: Proof of working principle of two-wavelength algorithm – successful recalculation of predefined concentration and temperature profiles.

Second, noise is added to the ideal deflection of red and blue light, which leads to a refractive index gradient for both wavelengths with a Gaussian noise distribution (best case), cf. figure 8. To be able to obtain proper results, it is important that the noise distributions of the two wavelength data are not totally independent. Figure 12 illustrates the result for an evaluation based on data with high correlation (correlation of 100 %) of the noise distribution for both wavelengths. In contrast, figure 13 shows the outcome for almost uncorrelated noise (correlation of 1 %) for both wavelengths.

It can be stated that a high correlation between the noise data is decision making for the success of the data evaluation. While the concentration and temperature profile presented in figure 12 are very close to the predefined, ideal data, the data evaluation fails for the case with low correlated noise data (figure 13). There might be two strategies to experimentally gain suitable data: first, it has to be guaranteed that the optical paths for the red and blue wavelength are identical (starting at light source, ending at camera). Second, if the first strategy is not sufficient, the absolute order of magnitude of noise must be reduced that much that low correlation of the noise data has no effect.

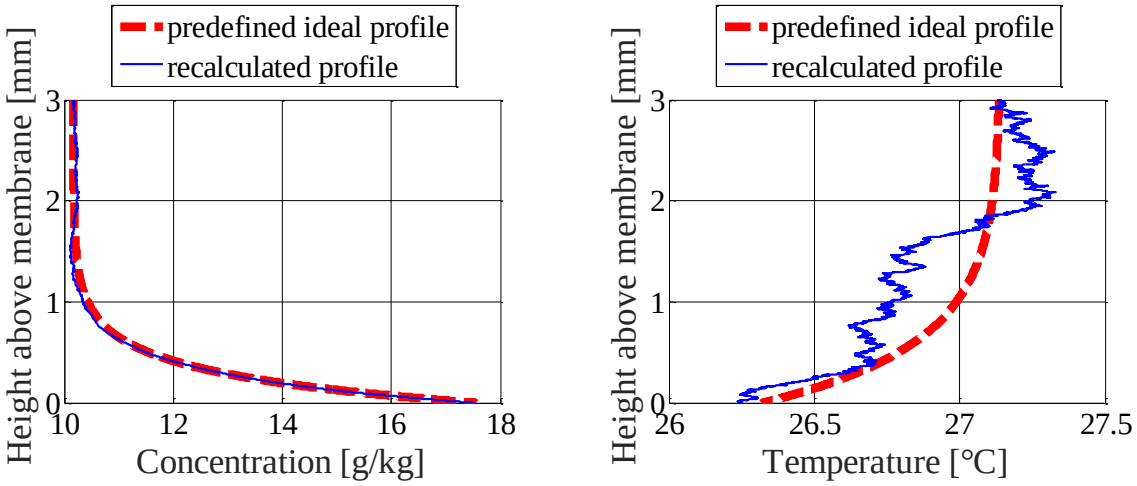

Figure 12: Proof of working principle of two-wavelength algorithm – evaluation with measurement noise for Schlieren (with high correlation between red and blue wavelength noise data).

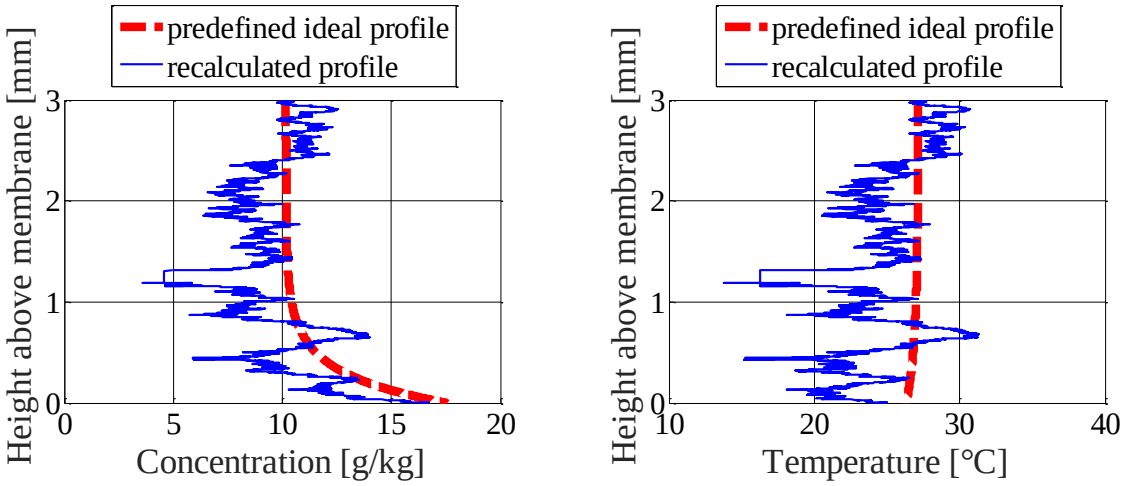

Figure 13: Proof of working principle of two-wavelength algorithm – evaluation with measurement noise for Schlieren (with low correlation between red and blue wavelength noise data).

4.2 Gradient Algorithm

The basic idea of the gradient algorithm was introduced in section 3.2. There, the equation of the refractive index gradient is derived applying a simple five-point backward finite differences scheme for both the concentration and temperature first-order derivative. The differences scheme, however, should be as accurate as possible as figure 14 and 15 indicate.

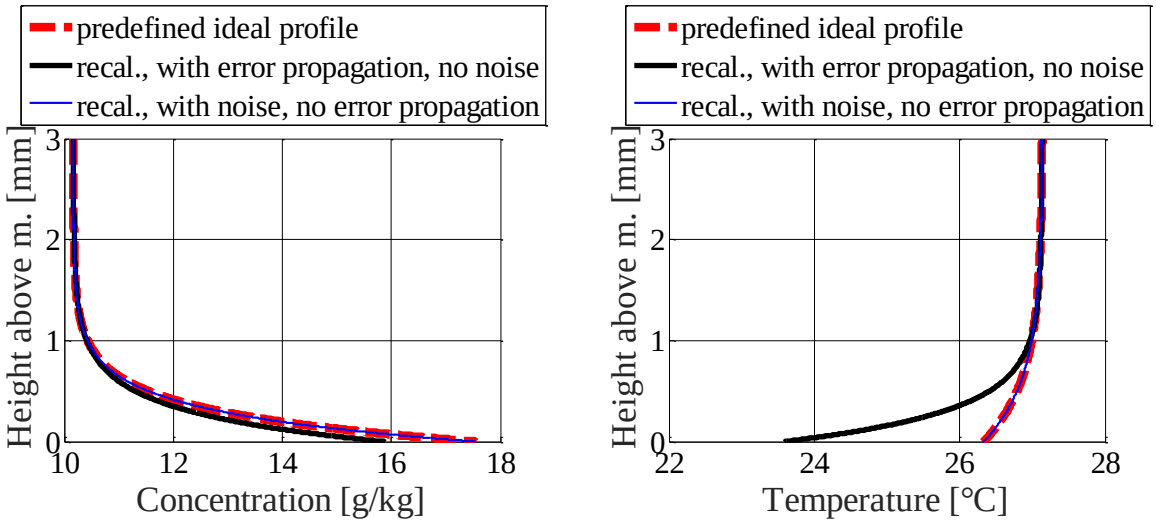

Figure 14: Investigation of working principle of gradient algorithm – recalculation (recal.) of concentration and temperature: poor results for the case with error propagation due to inaccurate differences scheme and promising results for the case without error propagation but with perturbation due to measurement noise (both results were obtained with 3000 discretization steps which corresponds to 3000 pixel of camera chip).

Figure 14 and 15 present the results for the re-calculation of the same concentration and temperature profile as described before (only the axis-scales in the diagrams were adjusted). In contrast to the results depicted in figure 11, the gradient algorithm shows comparably poor performance when reconstructing undisturbed data with a five-point backward differences scheme; the performance of a two-point differences scheme is even lower and not presented here. The reason might be the finite differences scheme itself.

Looking at the results for the re-calculation of the two profiles with measurement noise but without the error propagation caused by the inaccuracy of the temperature and concentration values due to the finite differences scheme (this is achieved by using ideal temperature and concentration values as input for backward data), the algorithm seems to work perfectly.

Thus, it can be concluded that the basic idea behind the gradient algorithm is valid. However, it has to be stated that the problem of error propagation due to the differences scheme might be a non-trivial problem to solve. The discretization step size cannot be increased further than the amount of pixels of the camera chip. A reduction of the truncation error by finding an appropriate differences scheme of even higher order might lead to the need of more than one initial value for temperature and concentration which have to be determined experimentally with sufficient accuracy. Assumed that this is successful, there is still the challenge of the influence of measurement noise on the refraction index and its gradient.

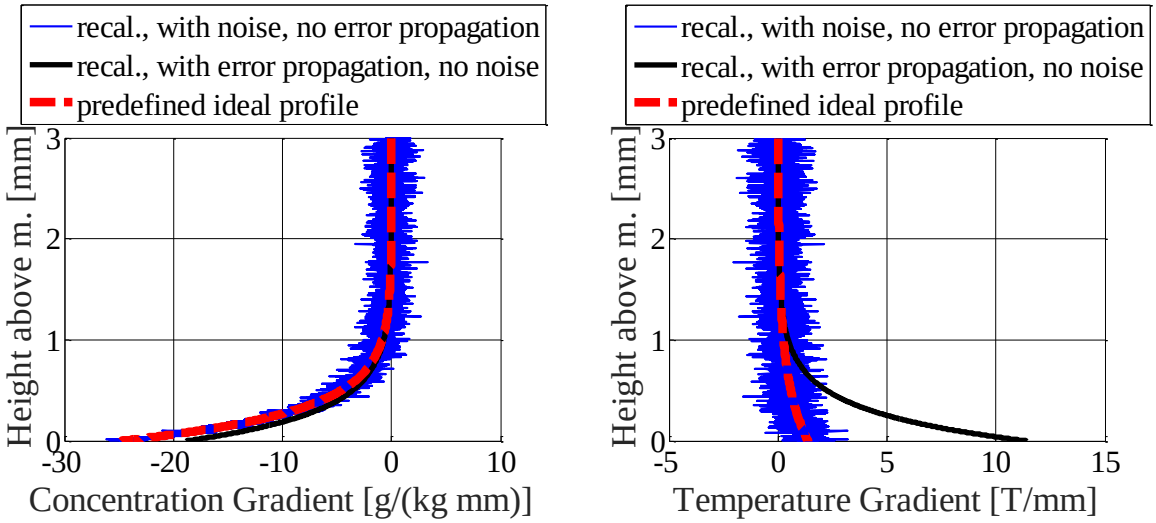

Figure 15: Investigation of working principle for gradient algorithm – recalculation (recal.) of concentration and temperature gradient: poor results for the case with error propagation due to inaccurate differences scheme and promising results for the case without error propagation but with perturbation due to measurement noise (both results were obtained with 3000 discretization steps).

4.3 Potential of proposed methods

The two-wavelengths Schlieren method has a high potential of being successful. It has been shown that the algorithm can handle the type of measurement noise, which occurs in Schlieren experiments. The weak point of the method turns out to be the need for high correlation between the measurement noises of the both wavelengths signals. This directly leads to an increased experimental effort in view of alignment and quality of optical components. A time-stable light source in view of wavelength spectrum and intensity, achromatic lenses, a double bandpass filter (in case of a white light source) and a temperature stabilized camera are recommended, just to give some examples. It is noted that the measurement noise applied in this paper is gained from experiments without a temperature stabilized camera, but a simple commercial single reflex camera, Canon EOS 700D.

From an experimental point of view, the combination of Schlieren and DHI makes sense to increase the overall measurement accuracy. Interesting is the finding, that both have the same order of magnitude for refraction index and refraction index accuracy. However, they show different trends of measurement accuracy what makes its combination quite interesting. As mentioned above, preliminary experiments with the DHI-Schlieren setup introduced in figure 5 showed that the alignment of the DHI part of the setup might become more difficult than in the DHI configuration without Schlieren (figure 4). It was expected that quantitative Laser-Schlieren with a gradient Schlieren filter might cause unwanted inference fringes in the recorded Schlieren image; this was not confirmed in the preliminary experiments: when investigation of boundary layers with thicknesses lower than 1 mm, magnification of the image of the investigated is required, which is helpful here; the magnification in the preliminary experiments was around 4.
In view of applying the gradient method to DHI or DHI-Schlieren, three problems still have to be solved: first, a suitable numerical difference scheme for the substitution of the analytical gradients of

temperature and concentration has to be found proving appropriate accuracy. Second, depending on the difference scheme, a certain amount of initial values for temperature and concentrations have to be derived experimentally with appropriate accuracy. Third, the order of magnitude of the measurement noise has to be determined which can still be handled by the gradient algorithm.
What seems to be rather unlikely is that DHI in combination with the gradient algorithm works. For this combination, a discretization step corresponding to the fringe positions was suggested before (section 3.2). Both, the discretization step as well as the differences scheme have a comparable, high influence on the accuracy of the numerical determination of the analytical gradients of temperature, concentration and also refraction index. In the analysis presented above, the number of discretization steps was chosen as high as possible and set to the maximum available pixels. The camera chip, for example, used in the preliminary experiments had a vertical resolution of 3000 pixels. The number of fringes appearing in the investigated concentration and temperature layers is significantly lower, about 3 to 30 with the DHI setup depending on the membrane operating conditions, just to give a rough approximation.

V. CONCLUSION AND OUTLOOK

Three methods were described to simultaneously measure heat and mass transfer in boundary layers with focus on membrane desalination. The methods were compared in view of measurement accuracy and applicability of post-processing algorithms for data evaluation. The two-wavelengths Schlieren method seems to have a high potential to be successfully applied in experiments. While single-wavelength DHI is unlikely to work in combination with the gradient method due to the poor discretization of measurement data, the applicability of Schlieren-DHI depends on the progress made in optimization of the gradient algorithm.

VI. ACKNOWLEDGEMENT

This work is part of the Joint German-Israeli Water Technology Research Program “PVT-RO” funded by the Federal Ministry of Education and Research (BMBF), Germany, and Ministry of Science and Technology (MOST), Israel.

VII. REFERENCES

1. Millard, R. C., Seaver, G., An index of refraction algorithm for seawater over temperature, pressure, salinity, density, and wavelength, Deep-Sea Research 37 (1990) no. 12, pp. 1909–1926.
2. Winter, D., Koschikowski, J., Wieghaus, M., Desalination using membrane distillation: experimental studies on full scale spiral wound modules, Journal of Membrane Science 375 (2011), pp. 104–112.
3. Martínez-Díez, L., Vázquez-González, M.I., Temperature and concentration polarization in membrane distillation of aqueous salt solutions, Journal of Membrane Science 156 (1999), pp. 265–273.
4. Kroiß, A., Spinnler, M., Sattelmayer, T., Method for determining local membrane parameters based on boundary layer investigations, IDA World Congress, 2015.
5. Chen, J., Li, Q., Menachem, E., In situ monitoring techniques for concentration polarization and fouling phenomena in membrane filtration, Advances in Colloid and Interface Science, 107 (2004), pp. 83–108.
6. Chen, V., Li, H., Fane, A.G., Non-invasive observation of synthetic membrane processes - a review of methods, Journal of Membrane Science, 241 (2004), pp. 23–44.

7. Vilker, V.L., Colton, C.K., Smith, K.A., Concentration polarization in protein ultrafiltration. Part I: an optical shadowgraph technique for measuring concentration profiles near a solution-membrane interface, AIChE Journal, 27 (1981), pp. 632–636.
8. Vilker, V.L., Colton, C.K., Smith, K.A., Concentration polarization in protein ultrafiltration. Part II: theoretical and experimental study of albumin ultrafiltered in an unstirred cell. AIChE Journal, 27 (1981), pp. 637–645.
9. Johnson, A.R., Experimental investigation of polarization effects in reverse osmosis. AIChE Journal, 20 (1974), pp. 966–974.
10. Mahlab, D., Yosef, N.B., Belfort, G., Interferometric measurement of concentration polarization profile for dissolved species in unstirred batch hyperfiltration (reverse osmosis), Chemical Engineering Communications, 6 (1980), pp. 225–243.
11. Clifton, M., Sanchez, V., Optical errors encountered in using Holographic Interferometry to observe liquid boundary layers in electrochemical cells. Electrochimica Acta, 24 (1979), pp. 445–450.
12. Fernández-Torres, M.J., Ruiz-Beviá, F., Fernández-Sempere, J., López-Leiva, M., Visualization of the UF polarized layer by Holographic Interferometry, AIChE Journal, 44 (1998), pp. 1765–1776.
13. Fernández-Sempere, J., Ruiz-Beviá, F., Salcedo-Díaz, R., Measurements by Holographic Interferometry of concentration profiles in dead-end ultrafiltration of polyethylene glycol solutions, Journal of Membrane Science, 229 (2004), pp. 187–197.
14. Fernández-Sempere, J., Ruiz-Beviá, F., Salcedo-Díaz, R., García Algado, P., Measurement of concentration profiles by Holographic Interferometry and modelling in unstirred batch reverse osmosis. Industrial & Engineering Chemistry Research, 45 (2006), pp. 7219–7231.
15. Fernández-Sempere, J., Ruiz-Beviá, F., Salcedo-Díaz, R., García-Algado, P., Diffusion studies in polarized reverse osmosis processes by Holographic Interferometry, Optics and Lasers in Engineering, 46 (2008), pp. 877–887.
16. Fernández-Sempere, J., Ruiz-Beviá, F., García-Algado, P., Salcedo-Díaz, R., Visualization and modelling of the polarization layer and a reversible adsorption process in PEG-10000 dead-end ultrafiltration, Journal of Membrane Science, 342 (2009), pp. 279–290.
17. Fernández-Sempere, J., Ruiz-Beviá, F., García-Algado, P., Salcedo-Díaz, R., Experimental study of concentration polarization in a crossflow reverse osmosis system using Digital Holographic Interferometry, Desalination, 257 (2010), pp. 36 – 45.
18. Salcedo Díaz, R. Aplicatión de la Interferometriía Holográfica al estudio de la capa de polarización en ósmosis inversa. Efecto de la convección natural, PhD thesis, Universidad de Alicante, 2006.
19. Rodrígues, C., Garcia-Algado, P., Semião, V., Norberta de Pinho, M., Geraldes, V., Concentration boundary layer visualization in nanofiltration by Holographic Interferometry with light deflection correction, Journal of Membrane Science, 447 (2013), pp. 306–314.
20 Beach, K.W., Muller, R.H., Tobias, C.W., Light-deflection effects in the interferometry of one-dimensional refractive-index fields, Journal of the Optical Society of America 63 (1973), no. 5, pp. 559–566.
21. Salcedo-Díaz, R., García-Algado, P., García-Rodrígues, M., Fernández-Sempere, J., Ruiz-Beviá, F., Visualization and modeling of the polarization layer in crossflow reverse osmosis in a slit-typ channel, Desalination 456 (2014), pp. 21–30.
22. Schnars, U., Jueptner, W., Digital Holography – digital hologram recording, numerical reconstruction, and related techniques, Springer Berlin Heidelberg New York, 2005.

23. Gowman, L., Ethier, R., Concentration and concentration gradient measurements in an ultrafiltration concentration polarization layer, Part I: A laser-based refractometric experimental technique, Journal of Membrane Science 131 (1997), pp. 95–105.
24. Prevosto, L., Artana, G., Mancinelli, B., Kelly, H., Schlieren technique applied to the arc temperature measurement in a high energy density cutting torch, Journal of Applied Physics 107 (2010), pp. 1–5.
25. Prevosto, L., Artana, G., Kelly, H., Mancinelli, B., Departures from local thermodynamic equilibrium in cutting arc plasmas derived from electron and gas density measurements using a two-wavelength quantitative Schlieren technique, Journal of Applied Physics 109 (2011), pp. 1–6.
26. Panknin, W., Eine holographische Zweiwellenlängen-Interferometrie zur Messung überlagerter Temperatur- und Konzentrationsgrenzschichten, PhD Thesis, Technical University of Hannover, 1977
27. El-Wakil, M.M., Ross, P.A., A two wavelength interferometric technique for the study of vaporization and combustion on fuels, liquid rockets and propellants, Progress in Astronautics and Rocketry 2 (1960).
28. Desse, J. M., Picart, P., Color holographic interferometry (from holographic plates to digital holography), 15th International Symposium on Flow Visualization, June 25-28, 2012, Minsk, Belarus.
29. Blue, R. E., Combination of Interferometer-Schlieren apparatus for density determination in non-homogeneous transparent fluids, United States Patent Office, 2,776,593, patented Jan. 8, 1957.
30. Kastell, D., Eitelberg, G., A combined Holographic Interferometer and Laser-Schlieren system applied to high temperature, high velocity flows, International Congress on Instrumentation in Aerospace Simulation Facilities, 18-21 July, Dayton, Ohio, USA (ICIASF 95 Record), 1995.
31. Tamburini A., Cipollina, A., Al-Sharif, S., Albeirutty, M., Gurreri, L., Micale, G., Ciofalo, M., Assessment of temperature polarization in membrane distillation channels by liquid crystal thermography, Desalination and Water Treatment (2014), pp. 1–19.
32. LCR Hallcrest Research & Testing Products, TLC coated polyester sheets, product information, www.lcrhallcrest.com, 2014.